Manuscript accepted for publication in the journal *Biomedical Signal Processing and Control*

Step Length Estimation with Wearable Sensors Using a Switched-Gain Nonlinear Observer

Ali Nouriani, Robert A. McGovern and Rajesh Rajamani

***Abstract*— This paper focuses on step length estimation using inertial measurement sensors. Accurate step length estimation has a number of useful health applications, including its use in characterizing the postural instability of Parkinson's disease patients. Three different sensor configurations are studied using sensors on the shank and/or thigh of a human subject. The estimation problem has several challenges due to unknown measurement bias, misalignment of the sensors on the body and the desire to use a minimum number of sensors. A nonlinear estimation problem is formulated that aims to estimate shank angle, thigh angle, bias parameters of the inertial sensors and step lengths. A nonlinear observer is designed using Lyapunov analysis and requires solving an LMI to find a stabilizing observer gain. It turns out that global stability over the entire operating region can only be obtained by using switched gains, one gain for each piecewise monotonic region of the nonlinear output function. Experimental results are presented on the performance of the nonlinear observer and compared with gold standard reference measurements from an infrared camera capture system. An innovative technique that utilizes three sensors is shown to provide a step length accuracy nearly equal to that of the four-sensor configuration.**

I. Introduction

Inertial measurement unit (IMU) sensors are widely used in navigation and stabilization systems. However, they suffer from measurement bias and drift that highly degrade the accuracy of integration-based position estimation algorithms in a short period of time after initialization. The unreliability of integration based position estimation from IMUs has been widely known for many years [1]. Therefore, IMUs are usually used in combination with other sensors like GPS, magnetometers or cameras. For example, Sukkarieh, et al. studied a combination of IMU and GPS signals through a Kalman Filter for a navigation application [2]. Wang and Rajamani estimated altitude by finding the direction cosine matrix using a combination of accelerometer and magnetometer measurements [3]. Since GPS satellite systems are not accurate enough for centimeter-level accuracy, IMUs have often been used with a combination of radar or camera systems in autonomous vehicle applications. For example, an IMU with Camera [4], an IMU-Lidar combination [5] and an IMU-GPS-Camera system [6] have been described in the literature. In addition, there are multiple papers that develop different stochastic filters to increase the accuracy and optimize the performance of these sensor combinations [7]–[9].

For the purpose of everyday human body motion tracking and step length estimation, GPS is not accurate enough and does not work well indoors. Camera systems are expensive, impractical to widely implement and raise many privacy concerns. Therefore, researchers have tried to find model-based methods to estimate body motions from IMUs. For instance, Matthews tried to solve a simplified three degree of freedom kinetic model of human gait using a Newton-Euler approach and simplifying assumptions on the internal body forces [10]. In another research study, Ketema and Gebre-Egziabher used a kinematic model of gait and presumed constraints on the gait pattern by assuming certain relations between the motions of the limbs to one another [11]. The problem with these approaches is they make several assumptions on the initial and boundary conditions and utilize gait constraints, which are not uniformly correct for different persons and situations. Weinberg used an empirical relation to calculate step lengths from accelerometers [12], Jahn, et al. compared some of these empirical and geometrical models with each other [13]. Davidson and Takala introduced a Kalman filter for estimation of velocity and step lengths from IMU acceleration measurements and compared its performance to empirical relations [14].

For estimation of the tilt angle and the measurement bias of IMUs we need nonlinear models and algorithms [15]. There are two major types of approaches in nonlinear observer design - high gain observers for triangular structure systems [16], [17] and linear matrix inequality based observers [18]. High gain observers are popular but have to address issues regarding noise sensitivity, high frequency model uncertainty and requirements on model structure [19]–[21]. On the other hand, LMI-based observers have been studied and developed for specific classes of nonlinear systems in the literature. For example, Wang developed LMI-based observers to handle nonlinear systems that have bounded Jacobians [22], Jeon introduced a gridded LMI-based observer for a nonlinear system with a wide range of operating conditions [23]. Rajamani et al. showed some important drawbacks of LMI-based observers for non-monotonic nonlinear systems and presented a solution by introducing a hybrid switched-gain observer [24].

A. Nouriani is a Ph.D. student in Mechanical Engineering at the University of Minnesota – Twin Cities, Minneapolis, MN 55455, USA. (e-mail: nouri011@umn.edu).

Robert McGovern is an Assistant Professor in the Department of Neurosurgery, University of Minnesota-Twin Cities, Minneapolis, MN 55455, USA. (e-mail: rmcgover@umn.edu)

R. Rajamani is a Professor of Mechanical Engineering at the University of Minnesota – Twin Cities, Minneapolis, MN 55455, USA. (e-mail: rajamani@umn.edu).

This research develops a hybrid switched-gain nonlinear observer for the step length estimation problem and presents a design based on solving a linear matrix inequality for each monotonic region in a nonlinear output function. The objective of this nonlinear observer is to estimate the real-time vertical in-plane angle of the IMU relative to the gravity vector as well as to estimate the real-time bias values of the accelerometer and gyroscope. The estimated real-time angle is used in finding the orientation of the body limb segment and also for transforming the accelerations to the inertial frame. This information is utilized in three different approaches for estimation of human step length:

i) The first method integrates the linear acceleration components of the shank sensors and provides the velocity and displacement of the sensors in space and hence the step lengths by assuming zero initial conditions at the start moment of each step. Only two sensors are needed.
ii) The second method estimates the orientations of multiple sensors and takes advantage of the geometry of the body to estimate step lengths. Four sensors (one on each shank and thigh) are needed.
iii) The third method utilizes only three sensors (one sensor on a thigh and two sensors on the two shanks) and assumes that each leg has a stance and swing phase during walking, with the thigh angular trajectory being symmetric between the two legs.

A preliminary version of these results was published in a conference paper [25]. This journal submission of the manuscript has the following additional contributions compared to the conference version:

a) This manuscript utilizes switched gains to ensure global stability of the observer over a large range of operating conditions for thigh and shank angles. The conference version had a constant observer gain, ensured only local stability, and only allowed limited operation over 0 to 30 degrees.

b) The conference version only had the two-sensor and four-sensor configurations while this manuscript proposes an innovative three-sensor configuration which is shown to provide almost the same level of accuracy as the 4-sensor configuration.

c) Complete proofs of all theoretical results are provided.

d) Significant additional experimental results are included here compared to the conference version of the paper.

In previous literature, there are three typical alternative methods for step length estimation:

1. Integration of accelerometer signals, but without calculation of tilt angles and without transformation of sensor-axes signals to inertial-axes signals. Fig 10 and 11 in this paper show the insufficiency of this method.

2. Estimation of the gravity vector using SO(3) attitude estimation methods. This type of approach is well established in the aerospace UAV community, e.g. [26], [27]. Some challenges in using this type of approach for wearable applications include the significant influence of local magnetic field disturbances due to ferromagnetic objects in the surroundings, and the conversion of a linear estimation problem into a nonlinear estimation problem when bias parameters are included in the plant model. While good estimation results with this type of estimation approach have been shown for UAV and other aerospace applications, there are less demonstrations of real-world performance in wearable medical applications.

3. Estimation with the same dynamic model presented in this paper but using stochastic approaches like the extended Kalman Filter (EKF), instead of using a nonlinear observer [11]. The disadvantages of the EKF for this application are the presence of non-monotonic nonlinear functions in the measurement equations which leads to poor robustness when there are model errors in the output nonlinear functions, as has been demonstrated by other publications in literature [28].

The remainder of this paper is organized as follows. In Section II, the nonlinear observer design algorithm is formulated. In Section III, three different step length estimation methods are described. In Section IV, experimental results for validating the accuracy of the nonlinear observer and the step length estimation methods are presented. Finally, section V presents the conclusions.

II. Nonlinear Observer

This paper assumes the use of either an IMU sensor on the shank (lower leg) or two IMU sensors, one each on the shank and thigh (upper leg), as shown in Fig.1. The axes of the IMU sensor and the attachment of it to a body limb segment are shown in Fig. 2. θ is the real-time absolute (inertial) angle of the limb segment and ψ is the unknown orientation angle of the sensor on the limb (due to small misalignments). Although ψ is unknown, it does not change with time, while the segment angle θ may continuously change with time. The sensor fixed axes are defined as (x, y) and the inertial frame fixed axes are (X, Y) as shown in Fig. 2. The variables a_x, a_y, a_X and a_Y are the true accelerations along these axes respectively.

Fig. 1. The mounting of the sensors on shank and thigh of the left leg.

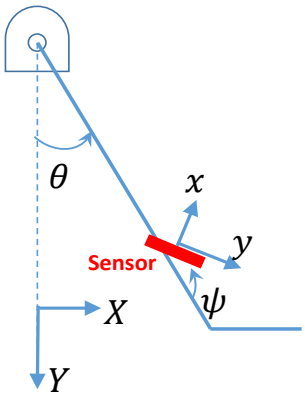

Fig. 2. The mounting and assumed axes of the sensor on a segment limb. The sensor is shown in red. Sensor-fixed axes are defined as (x, y) and the inertial frame axes are (X, Y) . θ is the real-time absolute (inertial) angle of the limb segment and ψ is the unknown mounting orientation angle of the sensor on the limb

A. Mathematical model

The orientation of each sensor is $\theta + \psi$, where θ is the real-time angle of the shank and ψ is the additional unknown mounting angle of the sensor on the shank.

Let

$$\phi = \theta + \psi. \tag{1}$$

Then the measurements of the accelerometers can be described by outputs y_1 and y_2:

$$y_2 = a_{ym} = a_y - g\cos(\phi) + b_{ay} \tag{2}$$

$$y_1 = a_{xm} = a_x - g\sin(\phi) + b_{ax} \tag{3}$$

The gyroscope signal measured by the sensor is described by the known input:

$$u = \omega_{gz} = \left(\dot{\theta} + \dot{\psi}\right)_{measured} = \dot{\theta} + b_{gz} \tag{4}$$

Here b_{ax}, b_{ay} and b_{gz} are the unknown bias values of the accelerometer and the gyroscope measurements and are assumed to be constant.

The relationships of the inertial accelerations to the sensor measured accelerations are given by:

$$a_X = a_x\cos(\theta + \psi) + a_y\sin(\theta + \psi) \tag{5}$$

$$a_Y = a_y\cos(\theta + \psi) - a_x\sin(\theta + \psi) \tag{6}$$

Then the overall dynamics of the sensor system on each lower leg can be described by the following equations:

$$\begin{aligned} \dot{\phi} &= \omega_{gz} + b_{gz} \\ \dot{b}_{ax} &= 0 \\ \dot{b}_{ay} &= 0 \\ \dot{b}_{gz} &= 0 \end{aligned} \tag{7}$$

In matrix form, the system dynamics are:

$$\frac{dx}{dt} = \frac{d}{dt}\begin{Bmatrix} \phi \\ b_{ax} \\ b_{ay} \\ b_{gz} \end{Bmatrix} = \begin{bmatrix} 0 & 0 & 0 & 1 \\ 0 & 0 & 0 & 0 \\ 0 & 0 & 0 & 0 \\ 0 & 0 & 0 & 0 \end{bmatrix}\begin{Bmatrix} \phi \\ b_{ax} \\ b_{ay} \\ b_{gz} \end{Bmatrix} + \begin{bmatrix} 1 \\ 0 \\ 0 \\ 0 \end{bmatrix}\omega_{gz} \tag{8}$$

$$y = \begin{Bmatrix} y_1 \\ y_2 \end{Bmatrix} = h(Ex) + Cx + DA_{input} \tag{9}$$

where

$$\begin{aligned} E &= [1 \quad 0 \quad 0 \quad 0] \\ C &= \begin{bmatrix} 0 & 1 & 0 & 0 \\ 0 & 0 & 1 & 0 \end{bmatrix} \\ A_{input} &= \begin{Bmatrix} a_x \\ a_y \end{Bmatrix} \end{aligned} \tag{10}$$

and

$$h(Ex) = \begin{Bmatrix} h_1(Ex) \\ h_2(Ex) \end{Bmatrix} = \begin{Bmatrix} -g\sin\phi \\ -g\cos\phi \end{Bmatrix}$$

In general system notation form, the system model is

$$\frac{d}{dt}x = Ax + B\omega_{gz} \tag{11}$$

$$y = Cx + h(Ex) + DA_{input} \tag{12}$$

B. Development of LMI-based observer design algorithm:

Let the observer be given as

$$\frac{d}{dt}\hat{x} = A\hat{x} + B\omega_{gz} + L\{y - C\hat{x} - h(E\hat{x})\} \tag{13}$$

Let the estimation error be:

$$\tilde{x} = x - \hat{x} \tag{14}$$

Then the estimation error dynamics are given by:

$$\dot{\tilde{x}} = \dot{x} - \dot{\hat{x}} = A\tilde{x} - LC\tilde{x} - Lh(Ex) + Lh(E\hat{x}) - LDA_{input}$$

or

$$\dot{\tilde{x}} = (A - LC)\tilde{x} - L\tilde{h}(Ex, E\hat{x}) - LDA_{input} \tag{15}$$

where $\tilde{h}(Ex, E\hat{x}) = h(Ex) - h(E\hat{x})$.

Lemma 1:

The nonlinear difference function $\tilde{h}(Ex, E\hat{x})$ satisfies the quadratic inequality

$$V_1 = [\tilde{x}^T \quad \tilde{h}(Ex, E\hat{x})^T]\,\Theta\begin{bmatrix} \tilde{x} \\ \tilde{h}(Ex, E\hat{x}) \end{bmatrix} \leq 0 \tag{16}$$

where

$$\Theta = \begin{bmatrix} \dfrac{E^T M^T NE + E^T N^T ME}{2} & -\dfrac{E^T M^T + E^T N^T}{2} \\ -\dfrac{ME + NE}{2} & I \end{bmatrix}$$

with $M = \begin{bmatrix} M_1 & 0 \\ 0 & M_2 \end{bmatrix}$ and $N = \begin{bmatrix} N_1 & 0 \\ 0 & N_2 \end{bmatrix}$ being diagonal matrices containing the lower and upper bounds on the partial derivates of $h_1(Ex) = -g\sin\phi$ and $h_2(Ex) = -g\cos\phi$ respectively.

Proof:

From the differential mean value theorem, $\exists\ z = Ex$ such that [25]

$$\tilde{h}(Ex, E\hat{x}) = \begin{Bmatrix} \vdots \\ h_i(Ex) - h_i(E\hat{x}) \\ \vdots \end{Bmatrix} = \begin{bmatrix} \left.\dfrac{\partial h_1}{\partial (Ex)}\right|_{z=z_1} & 0 & 0 & 0 \\ \vdots & \ddots & \ddots & 0 \\ 0 & & \ddots & 0 \\ 0 & \cdots & 0 & \left.\dfrac{\partial h_m}{\partial (Ex)}\right|_{z=z_m} \end{bmatrix} (Ex - E\hat{x}) \quad (17)$$

Then, using the lower and upper Jacobian bounds:

$$\tilde{h}(Ex, E\hat{x}) - ME\tilde{x} = \begin{bmatrix} \left.\dfrac{\partial h_1}{\partial (Ex)}\right|_{z=z_1} - M_1 & 0 & 0 & 0 \\ \vdots & \ddots & \ddots & 0 \\ 0 & & \ddots & 0 \\ 0 & \cdots & 0 & \left.\dfrac{\partial h_m}{\partial (Ex)}\right|_{z=z_m} - M_m \end{bmatrix} E\tilde{x} \quad (18)$$

and

$$\tilde{h}(Ex, E\hat{x}) - NE\tilde{x} = \operatorname{diag}\left\{ \left.\frac{\partial h_1}{\partial (Cx)}\right|_{z=z_1} - N_1, \dots\dots\dots, \left.\frac{\partial h_m}{\partial (Cx)}\right|_{z=z_m} - N_m \right\} E\tilde{x} \quad (19)$$

From (18) and (19), it follows that

$$\left[\tilde{h}(Ex, E\hat{x}) - ME\tilde{x}\right]^T \left[\tilde{h}(Ex, E\hat{x}) - NE\tilde{x}\right] = \tilde{x}^T E^T\ diag\left\{ \dots, \left(\left.\frac{\partial h_i}{\partial (Cx)}\right|_{z=z_i} - M_i \right)^T \left(\left.\frac{\partial h_i}{\partial (Cx)}\right|_{z=z_i} - N_i \right), \dots \right\} E\tilde{x} \quad (20)$$

Since each of the terms in the diagonal matrix is non-positive, the following negative definite inequality follows

$$\left[\tilde{h}(Ex, E\hat{x}) - ME\tilde{x}\right]^T \left[\tilde{h}(Ex, E\hat{x}) - NE\tilde{x}\right] \le 0 \quad (21)$$

Equation (21) can be rewritten as

$$[\tilde{x}^T \quad \tilde{h}(Ex, E\hat{x})^T] \begin{bmatrix} E^T M^T NE & -E^T M^T \\ -NE & I \end{bmatrix}^T \begin{bmatrix} \tilde{x} \\ \tilde{h}(Ex, E\hat{x}) \end{bmatrix} \le 0 \quad (22)$$

Since M and N can also be switched in (22), a symmetric form of (22) is

$$V_1 = [\tilde{x}^T \quad \tilde{h}(Ex, E\hat{x})^T] \begin{bmatrix} \frac{E^T M^T NE + E^T N^T ME}{2} & -\frac{E^T M^T + E^T N^T}{2} \\ -\frac{ME + NE}{2} & I \end{bmatrix} \begin{bmatrix} \tilde{x} \\ \tilde{h}(Ex, E\hat{x}) \end{bmatrix} \le 0 \quad (23)$$

QED.

Theorem 1:

If the acceleration input A_{input} is zero, then the errors in the estimates of the angle and the bias parameters will converge globally exponentially to zero, if the observer gain is selected so that the following LMI-equivalent inequality

$$S < 0 \quad (24)$$

yields a positive definite solution $P > 0$ and an observer gain solution L, with the elements of the matrix S defined as

$$s_{11} = (A - LC)^T P + P(A - LC) - \frac{E^T M^T NE + E^T N^T ME}{2} + \sigma P$$

$$s_{12} = -PL + \frac{E^T M^T + E^T N^T}{2}$$

$$s_{21} = -L^T P + \frac{ME + NE}{2}$$

$$s_{22} = -I.$$

Proof:

Consider the Lyapunov function candidate

$$V = \tilde{x}^T P \tilde{x} \quad (25)$$

with $P > 0$ being a positive definite matrix. Then

$$\begin{aligned} \dot{V} &= \dot{\tilde{x}}^T P\tilde{x} + \tilde{x}^T P\dot{\tilde{x}} \\ &= \tilde{x}^T[(A - LC)^T P + P(A - LC)]\tilde{x} \\ &\quad -\tilde{x}^T PL\tilde{h}(Ex, E\hat{x}) - \tilde{h}^T(Ex, E\hat{x})L^T P\tilde{x} \\ &\quad -\tilde{x}^T PLDA_{input} - A_{input}^T D^T L^T P\tilde{x} \end{aligned} \quad (26)$$

If $A_{input} = 0$, then

$$\begin{aligned} \dot{V} = \tilde{x}^T[(A - LC)^T P + P(A - LC)]\tilde{x} - \\ \tilde{x}^T PL\tilde{h}(Ex, E\hat{x}) - \tilde{h}^T(Ex, E\hat{x})L^T P\tilde{x} \end{aligned} \quad (27)$$

or $\dot{V} = [\tilde{x}^T \quad \tilde{h}(Ex, E\hat{x})^T] \begin{bmatrix} (A - LC)^T P + P(A - LC) & -PL \\ -L^T P & 0 \end{bmatrix} \begin{bmatrix} \tilde{x} \\ \tilde{h}(Ex, E\hat{x}) \end{bmatrix}$

Using the S-Procedure Lemma [29],

$\dot{V} < 0$ if and only if there exists $\epsilon > 0$ such that $\dot{V} \le \epsilon V_1$. Hence, $\dot{V} < 0$ if and only if

$$[\tilde{x}^T \quad \tilde{h}(Ex, E\hat{x})^T] \begin{bmatrix} (A - LC)^T P + P(A - LC) & -PL \\ -L^T P & 0 \end{bmatrix} \begin{bmatrix} \tilde{x} \\ \tilde{h}(Ex, E\hat{x}) \end{bmatrix} \le$$

$$\epsilon[\tilde{x}^T \quad \tilde{h}(Ex,E\hat{x})^T]\begin{bmatrix}\frac{E^TM^TNE+E^TN^TME}{2} & -\frac{E^TM^T+E^TN^T}{2}\\ -\frac{ME+NE}{2} & I\end{bmatrix}\begin{bmatrix}\tilde{x}\\ \tilde{h}(Ex,E\hat{x})\end{bmatrix}$$

or

$$S < 0 \tag{28}$$

where

$$s_{11} = \frac{(A-LC)^TP}{\epsilon} + \frac{P}{\epsilon}(A-LC) - \frac{E^TM^TNE+E^TN^TME}{2}$$

$$s_{12} = -PL/\epsilon + \frac{E^TM^T+E^TN^T}{2}$$

$$s_{21} = -\frac{L^TP}{\epsilon} + \frac{ME+NE}{2}$$

$$s_{22} = -I$$

Replacing P by a new positive definite matrix $P_1 = P/\epsilon$, and adding a σP term to the (1,1) entry for a guaranteed exponential convergence rate of $\sigma/2$, the result follows.

***Remark*:**

Low-pass filtered versions of y_1 and y_2 can be used in the observer so that the dynamic components are removed and A_{input} can indeed be negligible. In other words,

$$y_2 = a_{ym} = a_y - g\cos(\theta+\psi) + b_y$$
$$y_1 = a_{xm} = a_x - g\sin(\theta+\psi) + b_x$$

while

$$y_{2\_low\_pass} = -g\cos(\theta+\psi) + b_y$$
$$y_{1\_low\_pass} = -g\sin(\theta+\psi) + b_x$$

Hence, $\begin{Bmatrix}y_{1\_lowpass}\\ y_{2\_lowpass}\end{Bmatrix} = Cx + h(Ex)$, instead of $\begin{Bmatrix}y_1\\ y_2\end{Bmatrix} = Cx + h(Ex) + DA_{input}$, and thus $A_{input} = \begin{Bmatrix}a_x\\ a_y\end{Bmatrix} = 0$.

C. Hybrid observer using switched gains

It turns out that due to the output function for y_2, i.e. $h_2(Ex)$, being non-monotonic as shown in Fig. 3, the LMI (24) does not have a common feasible solution over the entire operating range of ϕ. Instead it is found to be feasible only in each of the monotonic regions R1, R2 and R3 shown in Fig. 3. This can be understood as follows:

The matrix A by itself is not stable for the given value of A in equations (8) – (10). When the nonlinear function $h(Ex)$ is non-monotonic, then the matrices M and N are diagonal matrices with $N > 0$ and $M < 0$. Hence the s_{11} element

$$s_{11} = (A-LC)^TP + P(A-LC) - \frac{E^TM^TNE+E^TN^TME}{2} + \sigma P$$

cannot be negative definite which rules out a feasible solution to the LMI (24). On the other hand, in each monotonic region M and N are both positive or negative definite (have the same sign). This enables a feasible solution to the LMI (24) in each monotonic region.

It is proved in [24] that a hybrid nonlinear observer which uses multiple constant-gain stable regions and switches between these stable gains with adequate dwell time after each switching is globally asymptotically stable. Thus, a single gain observer does not exist for the entire operating region and instead we need to solve equation (24) for each monotonic region of the nonlinear function h and find three different values of the observer gain. Then we switch between these 3 observer gains. Fig. 3 shows that in region 1 and region 3, both outputs are monotonic but in region 2 only the first output is monotonic. Therefore, the observers in region 1 and region 3 are designed based on both outputs and the observers in region 2 uses only the first output. Finally, a hybrid switching-gain observer with three constant gains is designed for the system. By solving the LMI of equation (24) using YALMIP in MATLAB, the three constant observer gains are obtained.

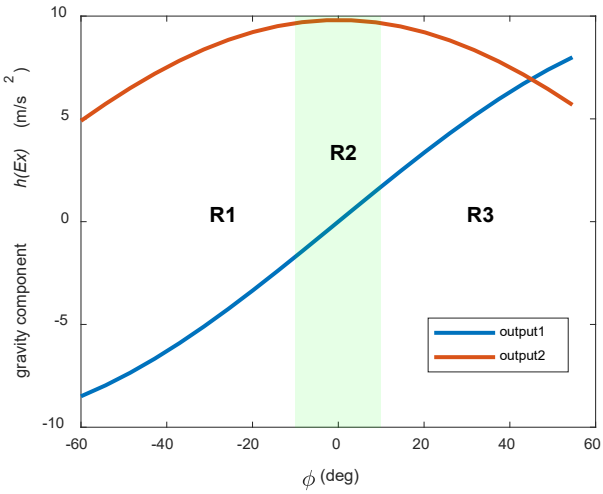

Fig. 3. Assumed constant-gain regions of the observer. In regions R1 and R3 both outputs are used but in region R2 only the first output is used.

III. Step Length Estimation

In this part three different methods are considered for estimating step lengths using configurations of two, three and four sensors respectively on the two legs of the subject.

I) In the first method, it is assumed that there are only two sensors (one attached to each shank) and an integrator-based method is used to estimate step length.
II) In the second method, we assume four sensors in all - one sensor on the shank and one on the thigh of each leg, and the estimated angles of both the shank and the thigh are used to find the step length.
III) In the third method, we assume there is one sensor attached to each shank and a third sensor is attached to one of the thighs.

A. Integrator-based estimation (two sensors configuration)

If there is only one sensor on each shank, we can find the step lengths based on the double-integration of the linear acceleration of the foot in the inertial frame. For this, we need to find the real-time orientation of the sensor relative to the

inertial frame and then transfer the corrected/unbiased accelerations (found from the nonlinear observer) using the following direction cosine matrix (DCM) to the inertial frame. Subsequently, the gravity component from the transformed accelerations need to be removed. Then the resulting dynamic accelerations are double integrated from the end of one step to the end of the next step. The DCM is given by:

$$R(\phi) = \begin{bmatrix} \cos(\phi) & -\sin(\phi) \\ \sin(\phi) & \cos(\phi) \end{bmatrix} \tag{29}$$

The relationship between inertial and sensor accelerations is given by

$$\begin{Bmatrix} a_X \\ a_Y \end{Bmatrix} = R(\phi) \begin{Bmatrix} a_x \\ a_y \end{Bmatrix} \tag{30}$$

The end of each is step is found based on the high peaks experienced in the RMS signal of each accelerometer. Fig. 4 shows that the end of each step has a clear local maximum in the RMS signal which is because of heel-strikes [10]. The start of integration is found based on the assumption of step-by-step walking. This means that the beginning of each step coincides with the end of the previous step. Experimental data has shown that starting integration earlier than the real lift off does not degrade accuracy because the foot is stationary. On the other hand, the accuracy degrades very fast if the integration is started late. In practice, therefore, we have seen good accuracy when we assume foot lift off happens at the end of the previous step.

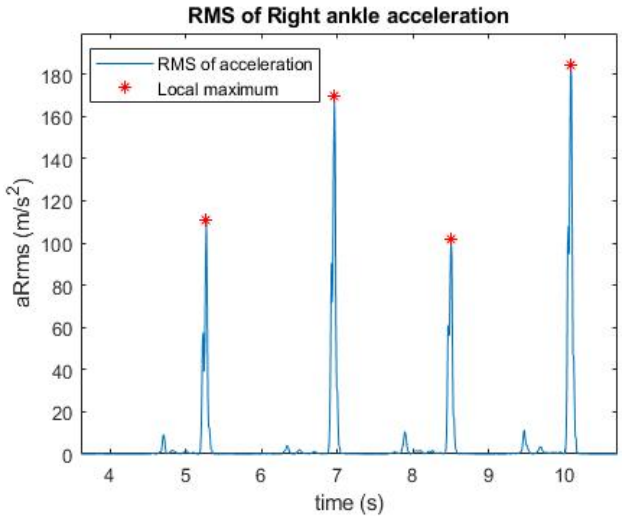

Fig. 4. An example of the RMS signal of the right shank acceleration and its local maximums that are used to identify the heel-strikes of each step

B. *Angle-based estimation (four sensors configuration)*

Another method is to estimate the step lengths from the geometry of the body during in-plane walking. Fig. 5 shows a schematic model of the body and the angles of each limb. In this method we need to use four sensors, one sensor on each shank and thigh to be able to estimate the angles of both shank and thigh in real-time. Based on Fig. 5 we can calculate the real-time relative position of the feet using the following simple trigonometric equations and so find the step lengths at the end of each step. For example, assume that the right foot is on the ground and the left leg is swinging then we have the position of right foot relative to the left foot as:

$$\begin{aligned} X_{r/l} = {} & L_{sr}\sin(\theta_{sr}(t)) + L_{tr}\sin(\theta_{tr}(t)) \\ & + L_{sl}\sin(\theta_{sl}(t)) + L_{tl}\sin(\theta_{tl}(t)) \end{aligned} \tag{31}$$

$$\begin{aligned} Y_{r/l} = {} & L_{sl}\cos(\theta_{sl}(t)) + L_{tl}\cos(\theta_{tl}(t)) \\ & - L_{sr}\cos(\theta_{sr}(t)) - L_{tr}\cos(\theta_{tr}(t)) \end{aligned} \tag{32}$$

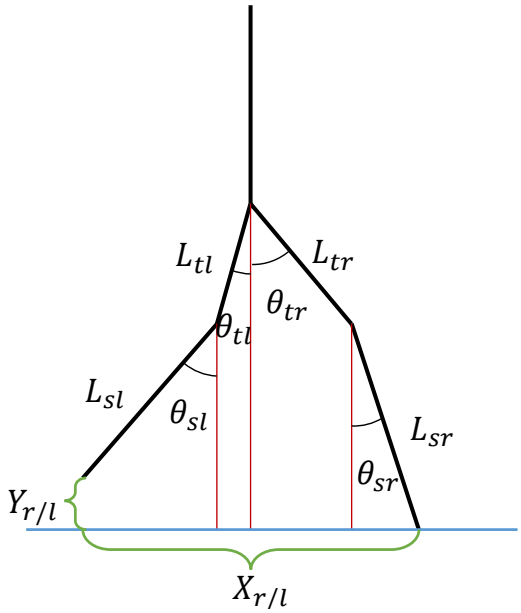

Fig. 5. Schematic of body during in-plane walking. The angles of right shank, right thigh, left shank, and left thigh with vertical axis are shown as θ_{sr}, θ_{tr}, θ_{sl}, and θ_{tl} respectively. Also the length of right shank, right thigh, left shank, and left thigh are L_{sr}, L_{tr}, L_{sl}, and L_{tl} respectively.

The time of end of each step is found from the high peaks experienced in the RMS signal of each accelerometer as discussed in the previous section and shown in Fig 4. If we assume that we detect an end of step in the left foot, the step length is therefore computed as below:

$$\begin{aligned} Step\ length = {} & L_{sr}\sin(\theta_{sr}(t_{el})) + L_{tr}\sin(\theta_{tr}(t_{el})) \\ & + L_{sl}\sin(\theta_{sl}(t_{el})) + L_{tl}\sin(\theta_{tl}(t_{el})) \end{aligned} \tag{33}$$

in which t_{el} is the time at the end of left foot step.

C. *Polynomial angle-based estimation (three sensors configuration)*

In this method, we utilize only one of the thigh sensors and estimate the angle of the other thigh by a polynomial function of time, based on the first leg's thigh angle and then use Eq. (33) again to estimate the step lengths from the geometry of in-plane walking.

We divide walking into the two main parts of swing and stance phases based on the angles of the thigh and shank as shown in Fig. 6. During the stance phase, the foot is on the

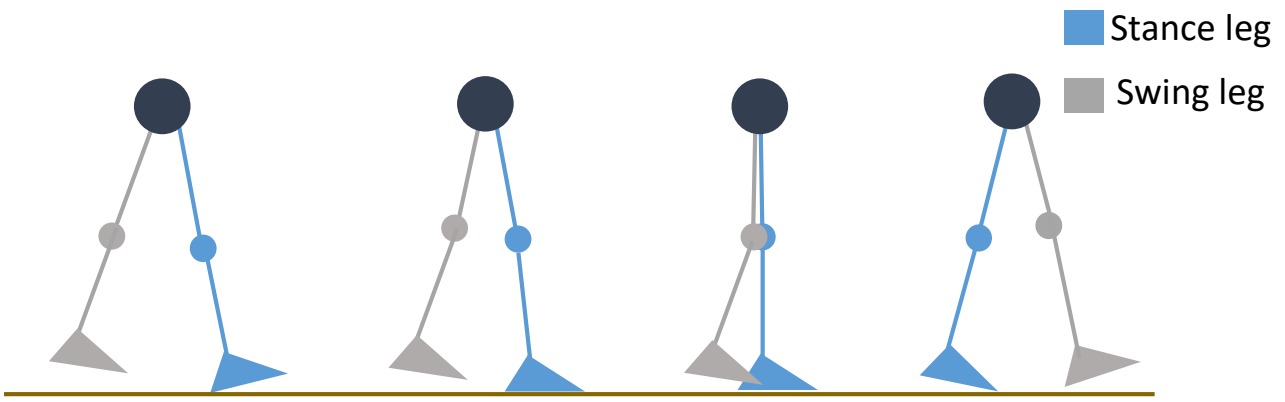

Fig. 6. Schematic of swing and stance phases of walking. During stance phase, the foot is on the ground and the thigh angle of the swing leg is almost equal to the shank angle. During swing phase, foot is swinging in the air and the thigh angle diverges from shank angle.

ground and the angle of the shank and thigh are almost equal (shank and thigh are aligned). However, during the swing phase, the leg is swinging in the air and the angle of thigh diverges from that of the shank.

For the swing phase we estimate the thigh angle from a polynomial fitted to the swing phase angle of the other leg as described below:

1) Estimate left thigh angle $\widehat{\theta}_{tl}$ using the nonlinear observer described in equation (13) since we have IMU on the left thigh.

2) Fit a 4th order polynomial to the estimated left thigh angle $\hat{\theta}_{tl}$ using least squares:

$$\widehat{\theta}_{tl}(t) = p_4 t^4 + p_3 t^3 + p_2 t^2 + p_1 t + p_0 \qquad (34)$$

in which t shows time, p_i are the polynomial coefficients found from a least squares solution, and θ_{tl} is the estimated left thigh angle.

3) Estimate the right thigh angle using the calculated polynomial by shifting the time relative to the start of the right footstep.

$$\widehat{\theta}_{tr}(t) = p_4(t - t_{sr})^4 + p_3(t - t_{sr})^3 + p_2(t - t_{sr})^2 + p_1(t - t_{sr}) + p_0 \qquad (35)$$

in which t_{sr} shows the start time of the right footstep.

Fig. 7 shows the angles of shank and thigh of both legs during stance and swing phase. The shank angles of both left and right legs, and the thigh angle of the left leg are estimated from the nonlinear observer. The thigh angle of the right leg is assumed to be equal to the shank angle during stance phase, however during swing phase it is estimated by a polynomial fitted using least squares to the left leg thigh angle estimates. This figure shows that we can estimate the right thigh angle successfully by this method.

IV. Experimental Results

Inexpensive commercial Inertial Measurement Units (IMUs) made by MbientLab Inc. are used as the measurement sensors. Each device has a 32-Bit ARM Cortex M4F processor powered by a high capacity CR2450 Lithium Coin Cell. The internal measurement sensor is a Bosch BMI160 consisting of a three-axis accelerometer and a three-axis gyroscope [30]. The data from the IMU is sampled at a 100Hz frequency and

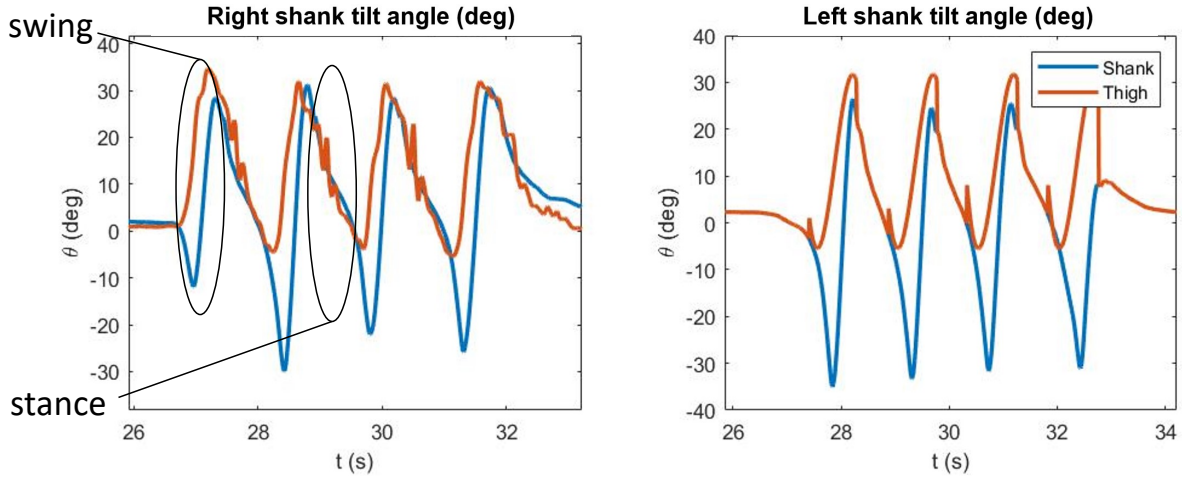

Fig. 7. Angles of shank and thigh of both legs during stance and swing phase. Both angles of left leg and shank angle of right leg are from nonlinear observer. The thigh angle of the right leg is assumed to be equal to the shank angle during stance phase, however during swing phase it is estimated by a polynomial fitted using least squares to the left leg estimates.

stored on a flash memory and also could be streamed through Bluetooth connectivity to a smartphone or computer. The IMU and its sensor-fixed frame are shown in Fig. 8.

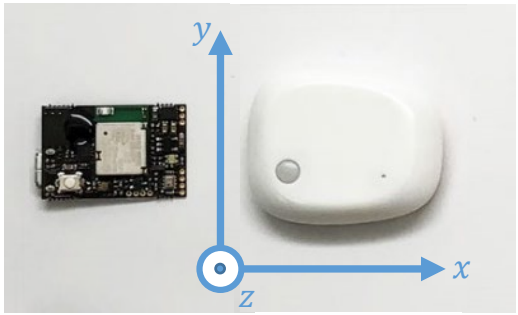

Fig. 8. Inertial measurement unit board, case and its sensor-fixed frame.

The experiments were performed on one healthy subject with IRB approval. The sensors were mounted on the subject as shown in Fig. 1. Since the experiment is not designed to study a medical hypothesis, multiple subjects were not recruited. There was no special effort made to align the sensors. The alignment of the sensor is automatically compensated for by the estimation algorithms. The experiments are designed to demonstrate the performance of the estimation algorithm in comparison to a gold standard infrared camera measurement system.

An IR motion tracking camera is used as an accurate reference sensor with which the estimated step lengths and angles from the nonlinear observer are compared. The IR camera setup is an OptiTrack V120:Trio model which is a self-contained and factory calibrated camera and uses three cameras and built-in software to track passive markers attached to the body with sub-millimeter accuracy. The sample rate of the camera system is 120 Hz [31]. The experiments were performed on one healthy subject with IRB approval.

Tests were conducted consisting of walking and stumbling in both forward and backward directions to observe the accuracy of the estimations in both low and high acceleration motions. The term "stumbling" means simulation of near-fall activities. Stumbling was included in addition to walking in order to show that our algorithm works in the presence of disturbances and to prepare for other future studies. The first 30 seconds of the test is walking, and the rest of the test data consists of walking and stumbling.

An optimum value of $\sigma = 0.45$ for the convergence rate was found numerically to yield the minimum estimation error. We can compare the overall accuracy of the shank angle estimation of the nonlinear observer with the IR camera measurements in Fig. 9. It can be seen that the shank angle estimates track the IR camera angle estimates very closely.

To show the effect and the importance of the nonlinear observer on estimation of the step lengths we plotted the direct double integration of the raw IMU acceleration measurement to find foot displacement in Fig.10.

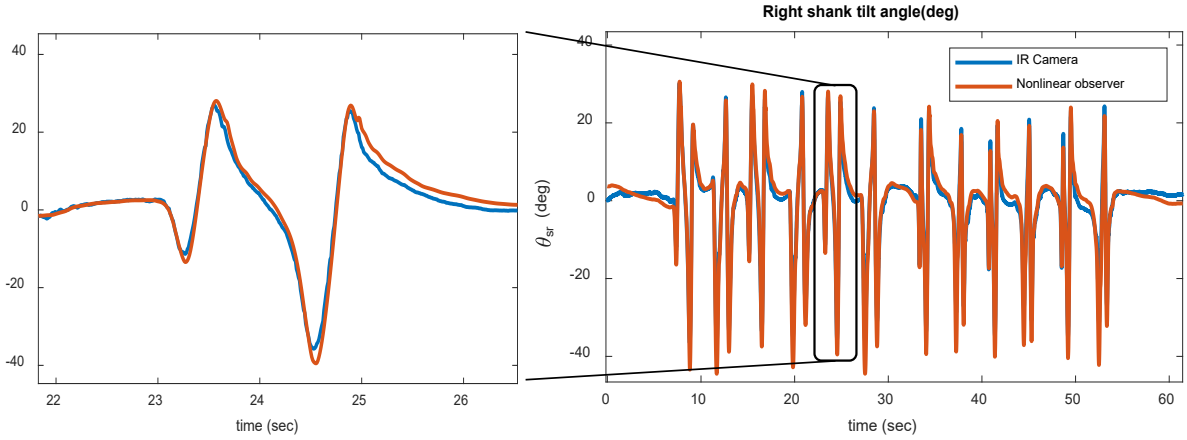

Fig. 9. Right shank tilt angle from IR camera and nonlinear observer.

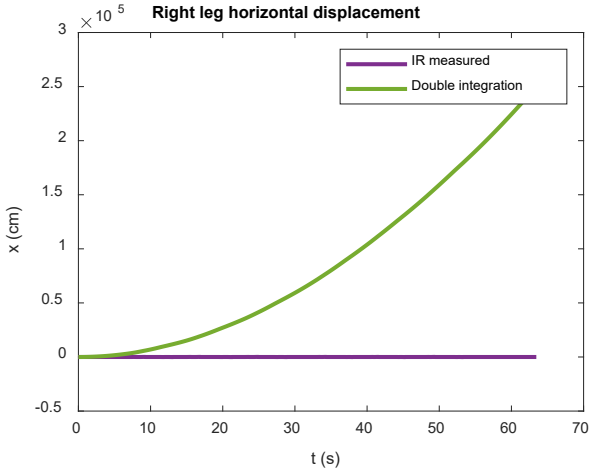

Fig. 10. Right leg horizontal displacement from IR camera and direct double integration of IMU acceleration measurements.

Also, the tilt angles from direct integration of gyro measurements are compared to IR camera measurements in Fig. 11. As the figures show, the direct integration of gyro has a linear growing drift while double integration of accelerations results in an exponential growing position drifts due to not

having removed the bias and tilt angle errors in IMU measurements.

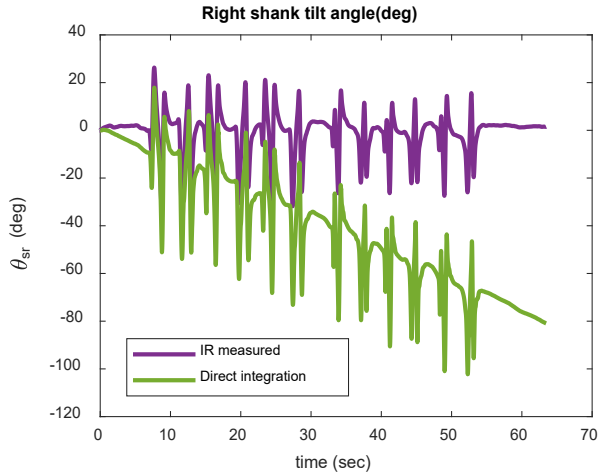

Fig. 11. Right shank tilt angle from IR camera and direct integration of IMU gyro measurements.

Fig. 12 shows a comparison of step length estimation of all three observer-based methods with the IR camera. Based on the shown results the average accuracy of the two-sensor integrator-based method is found to be 91.42%, for the three-sensor angle-based method is 94.64% and for the four-sensor angle based is 95.67%. The reason for this difference is that the integrator-based method depends on the initial conditions and measurement biases with high sensitivity because of double integration while the angle-based method uses the real-time estimation of the angles and is independent of initial conditions and much less influenced by the bias errors. Also the reason for the difference between four and three sensor methods is that the three sensor method relies on a polynomial for the estimation of right thigh angle while the four sensor method estimates it by the nonlinear observer from direct measurement of all 4 IMUs.

The latter 30 second of the test includes the stumbling part of the test. In this part, we see more errors, especially in the integration mode. The average step length error in the second half of the test is 5.93% for the four-sensor angle-based method while it is 10.34% for the three sensor and 26.32% for the integrator-based method. Again, the integration mode shows more sensitivity to the initial conditions and errors due to the impulses during stumbling. Also, the polynomials become less accurate due to differences between walking and stumbling.

The estimated bias from the nonlinear observer is shown for the horizontal axis accelerations in Fig. 13. This estimation shows that the bias changes as the foot accelerates and decelerates which makes sense since micro-electro-mechanical sensors are known to have slow time-varying drift in the bias [1].

Fig. 14 shows the tilt angle error obtained by taking the difference between the estimated angle of the nonlinear observer and the reference value from the IR camera. The IR camera data is exported to 100 Hz sample rate using OptiTrack built-in software and synchronized to the IMU data using MATALB cross correlation tools. The maximum angle error is about 2 degrees over the range of -40 to +30 degrees which is an acceptable error using inexpensive IMUs. Therefore, the maximum error rate is 2.86% in the walking part. The second part of the test (stumbling) shows higher peaks and maximum angle error is 3 degrees which shows about 4.29% max error in the stumbling part.

The horizontal position estimation error of the right foot for the methods of two, three and four sensor estimation computed by comparing with the IR camera are shown in Fig. 15. The angle mode obviously has superior accuracy relative to the integration mode in this figure. The maximum error is 3.54 cm (7.63%) for the 4-sensor mode and 5.12 cm (12.81%) for the 3-sensor mode. On the other hand, the maximum error is 11.34 cm (28.35%) for the 2-sensor integration mode. The maximum error becomes smaller if we neglect the stumbling part of the test. Maximum error is 2.94 cm (6.67%) for the 4-sensor angle mode and 3.97 cm (8.94%) for the 3-sensor mode, while the max error is 9.43 cm (19.52%) for the integration mode in just the first part of the test.

V. Conclusions

This paper has presented three step length estimation approaches using a nonlinear switched-gain observer based on measurements from IMUs worn on leg segments. The observer estimates the orientation and measurement bias of each IMU. A switched-gain strategy is used for the observer in which three piecewise working regions are utilized in each of which the output function is monotonic. The orientation of the sensor and measurement bias are estimated in real-time, the bias and gravity components are removed from it to find the true linear accelerations, and then the accelerations are transformed to the inertial frame. Using this observer, three different approaches are presented for the step length estimation. First, we assumed the use of sensors only on each shank and the step lengths are found by integration of the linear inertial-frame accelerations of each leg from the start to the end of each step. In the second approach, we assume there is one sensor attached to each shank and a third sensor is attached to one of the thighs. In the third method, we assume each leg has two sensors, one sensor on the shank and one on the thigh, and the step length is estimated using the estimated angles of the limb segments and the geometry of the body posture. The second method which utilizes a sensor in only one of the two thighs utilizes an innovative approach to estimate the orientation angle of the other thigh by assuming symmetric motion between thighs during the swing phase.

The results of these estimators are compared to results from an expensive IR camera motion capture system by performing tests of walking and stumbling in the forward and backward directions. The results show that the angles of the limbs are estimated very accurately, as verified by the IR camera. The integrator-based method is a simpler strategy and needs less resources due to the low number (just 2) of sensors. However, the angle-based method shows better accuracy in terms of step length estimation since it is not sensitive to the

initial conditions and errors caused by double integration. The four-sensor method uses two sensors for the thighs and estimates both thigh angles from measurement of IMUs while the three-sensor configuration estimates the thigh angle of one foot by fitting a polynomial to the estimated angle of the other foot. The three-sensor method shows comparable accuracy to the four-sensor mode while it does fall a little behind during more disturbances in stumbling experiments. Further, the accuracy of the three-sensor method may also fall when the gait of the subject is non-symmetric.

The developed nonlinear switched-gain observer can be a powerful tool in the estimation of the orientation angles and bias values of IMU sensors which have many problems in general with drifts and errors. This method has the potential to be applied wherever IMUs are employed including navigation and stabilization problems. Two step length estimators are introduced as successful applications of this observer. These step estimators could help us monitor activity and health of ordinary people, as well as of athletes and patients.

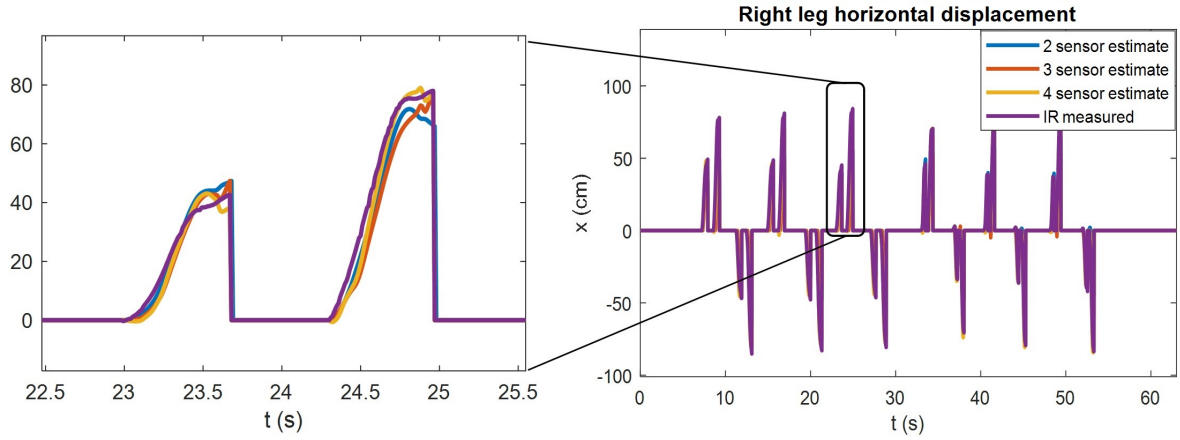

Fig. 12. Right leg horizontal displacement from IR camera and nonlinear observer in integrate and angle modes.

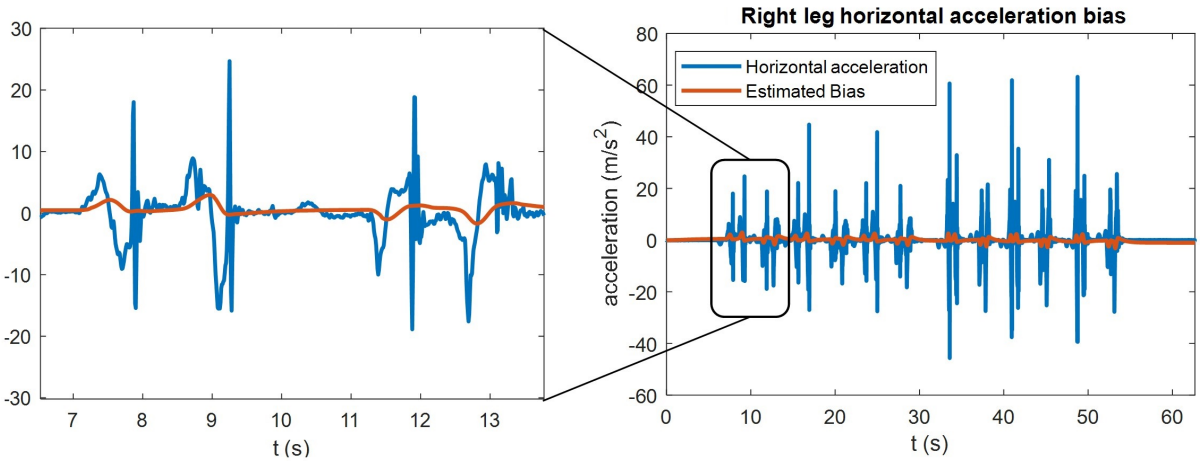

Fig. 13. Estimated right leg accelerometer horizontal bias using nonlinear observer.

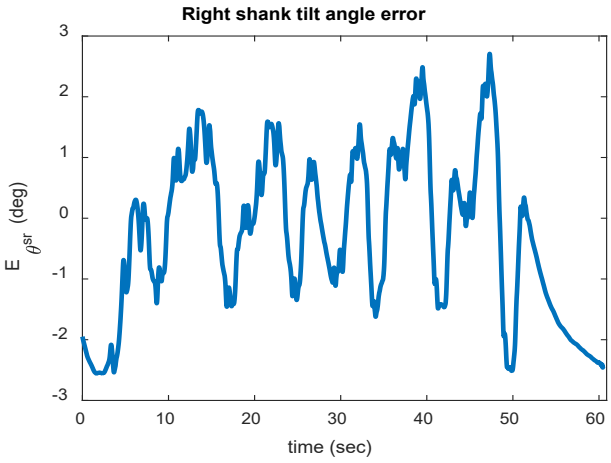

Fig. 14. Right leg tilt angle error of nonlinear observer compared to the IR camera measurement.

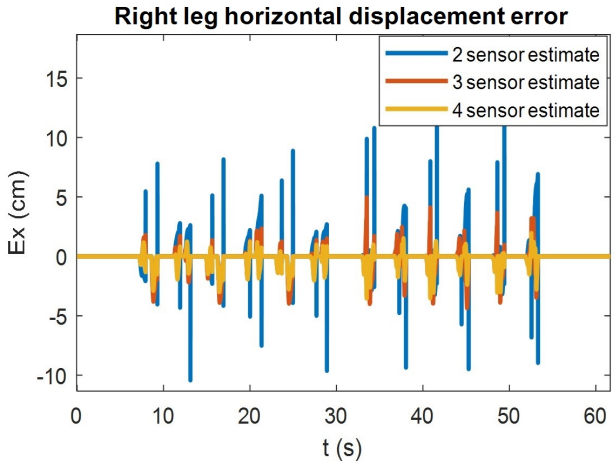

Fig. 15. Right leg horizontal displacement error in both integration and angle modes. First 30 seconds show normal walking and the second half shows stumbling.

REFERENCES

[1] J. C. Hung, J. R. Thacher, and H. V. White, "Calibration of accelerometer triad of an IMU with drifting Z-accelerometer bias," in *IEEE Proceedings of the National Aerospace and Electronics Conference*, 1989, vol. 1, pp. 153–158.

[2] S. Sukkarieh, E. M. Nebot, and H. F. Durrant-Whyte, "A high integrity IMU/GPS navigation loop for autonomous land vehicle applications," *IEEE Transactions on Robotics and Automation*, vol. 15, no. 3, pp. 572–578, 1999.

[3] Y. Wang and R. Rajamani, "Direction cosine matrix estimation with an inertial measurement unit," *Mechanical Systems and Signal Processing*, vol. 109, pp. 268–284, Sep. 2018.

[4] A. A. M. Assidiq, O. O. Khalifa, M. R. Islam, and S. Khan, "Real time lane detection for autonomous vehicles," in *Proceedings of the International Conference on Computer and Communication Engineering 2008, ICCCE08: Global Links for Human Development*, 2008, pp. 82–88.

[5] C. Rose, J. Britt, J. Allen, and D. Bevly, "An integrated vehicle navigation system utilizing lane-detection and lateral position estimation systems in difficult environments for GPS," *IEEE Transactions on Intelligent Transportation Systems*, vol. 15, no. 6, pp. 2615–2629, Dec. 2014.

[6] T. Chu, N. Guo, S. Backén, and D. Akos, "Monocular Camera/IMU/GNSS Integration for Ground Vehicle Navigation in Challenging GNSS Environments," *Sensors*, vol. 12, no. 3, pp. 3162–3185, Mar. 2012.

[7] A. Fakharian, T. Gustafsson, and M. Mehrfam, "Adaptive Kalman filtering based navigation: An IMU/GPS integration approach," in *2011 International Conference on Networking, Sensing and Control, ICNSC 2011*, 2011, pp. 181–185.

[8] Q. Xu, X. Li, and C.-Y. Chan, "A Cost-Effective Vehicle Localization Solution Using an Interacting Multiple Model−Unscented Kalman Filters (IMM-UKF) Algorithm and Grey Neural Network," *Sensors*, vol. 17, no. 6, p. 1431, Jun. 2017.

[9] Y. Liu, X. Fan, C. Lv, J. Wu, L. Li, and D. Ding, "An innovative information fusion method with adaptive Kalman filter for integrated INS/GPS navigation of autonomous vehicles," *Mechanical Systems and Signal Processing*, vol. 100, pp. 605–616, Feb. 2018.

[10] C. J. Matthews, "Personal Navigation Using a Kinetic Model of Human Gait," M.S. Thesis, Aerospace Engineering and Mechanics Department, University of Minnesota, Twin-cities, 2010.

[11] Y. Ketema and D. Gebre-Egziabher, "Experimentally Derived Kinetic Model for Sensor-Based Gait Monitoring," *Journal of Biomechanical Engineering*, vol. 138, no. 1, Jan. 2016.

[12] H. Weinberg, "Using the ADXL202 in Pedometer and Personal Navigation Applications," 2002.

[13] J. Jahn, U. Batzer, J. Seitz, L. Patino-Studencka, and J. G. Boronat, "Comparison and evaluation of acceleration based step length estimators for handheld devices," in *2010 International Conference on Indoor Positioning and Indoor Navigation, IPIN 2010 - Conference Proceedings*, 2010.

[14] P. Davidson and J. Takala, "Algorithm for pedestrian navigation combining IMU measurements and gait models," *Gyroscopy and Navigation*, vol. 4, no. 2, pp. 79–84, Apr. 2013.

[15] G. G. Scandaroli and P. Morin, "Nonlinear filter design for pose and IMU bias estimation," in *Proceedings - IEEE International Conference on Robotics and Automation*, 2011, pp. 4524–4530.

[16] H. K. Khalil and L. Praly, "High-gain observers in nonlinear feedback control," *International Journal of Robust and Nonlinear Control*, vol. 24, no. 6, pp. 993–1015, Apr. 2014.

[17] H. K. Khalil, *Nonlinear control*. Pearson Education, 2015.

[18] A. Zemouche, R. Rajamani, G. Phanomchoeng, B. Boulkroune, H. Rafaralahy, and M. Zasadzinski, "Circle criterion-based $\mathscr{H}\infty$ observer design for Lipschitz and monotonic nonlinear systems – Enhanced LMI conditions and constructive discussions," *Automatica*, vol. 85, pp. 412–425, Nov. 2017.

[19] V. Andrieu, L. Praly, and A. Astolfi, "High gain observers with updated gain and homogeneous correction terms," *Automatica*, vol. 45, no. 2, pp. 422–428, Feb. 2009.

[20] N. Boizot, E. Busvelle, and J. P. Gauthier, "An adaptive high-gain observer for nonlinear systems," *Automatica*, vol. 46, no. 9, pp. 1483–1488, Sep. 2010.

[21] J. H. Ahrens and H. K. Khalil, "High-gain observers in the presence of measurement noise: A switched-gain approach," *Automatica*, vol. 45, no. 4, pp. 936–943, Apr. 2009.

[22] Y. Wang, R. Rajamani, and D. M. Bevly, "Observer Design for Parameter Varying Differentiable Nonlinear Systems, with Application to Slip Angle Estimation," *IEEE Transactions on Automatic Control*, vol. 62, no. 4, pp. 1940–1945, Apr. 2017.

[23] W. Jeon, A. Zemouche, and R. Rajamani, "Tracking of Vehicle Motion on Highways and Urban Roads Using a Nonlinear Observer," *IEEE/ASME Transactions on Mechatronics*, vol. 24, no. 2, pp. 644–655, Apr. 2019.

[24] R. Rajamani, W. Jeon, H. Movahedi, and A. Zemouche, "On the need for switched-gain observers for non-monotonic nonlinear systems," *Automatica*, vol. 114, p. 108814, Apr. 2020.

[25] A. Nouriani, R. McGovern, and R. Rajamani, "Step Length Estimation Using Inertial Measurements Units," in *Proceedings of the 2021 American Control Conference (ACC), May 25-28,* New Orleans, USA, 2021.

[26] H. No, A. Cho, and C. Kee, "Attitude estimation method for small UAV under accelerative environment," *GPS Solutions*, vol. 19, no. 3, pp. 343–355, Jul. 2015.

[27] C. Eling, L. Klingbeil, and H. Kuhlmann, "Real-time

single-frequency GPS/MEMS-IMU attitude determination of lightweight UAVs," *Sensors*, vol. 15, no. 10, pp. 26212–26235, Oct. 2015.

[28] H. Movahedi, M. A. Figueroa-Santos, J. B. Siegel, A. G. Stefanopoulou, and R. Rajamani, "Hybrid nonlinear observer for battery state-of-charge estimation using nonmonotonic force measurements," *Advanced Control for Applications: Engineering and Industrial Systems*, vol. 2, no. 3, p. 38, Jul. 2020.

[29] S. Boyd, L. El Ghaoui, E. Feron, and V. Balakrishnan, *Linear matrix inequalities in system and control theory*. Society for Industrial and Applied Mathematics, SIAM Studies in Applied Mathematics, 1994.

[30] "Metamonitor r0.3 Product datasheet v0.5," 2017. [Online]. Available: https://mbientlab.com/documents/MetaMotionR-PS3.pdf. [Accessed: 29-Aug-2020].

[31] "OptiTrack V120 Duo & Trio Datasheet," 2018. [Online]. Available: www.optitrack.com. [Accessed: 29-Aug-2020].